Supporting Information

Spectroscopy-guided optimization of copper-based catalysts for low-temperature CO2 recycling to CO

Rubén Blay-Roger[1,*], Vincent Blay[2], Guillermo Torres Sempere[1], Nuria García-Moncada[1,3], Tomas Ramirez Reina[1], Bertrand Lacroix[1], Luis F. Bobadilla[1], José A. Odriozola[1,4]

[1] Inorganic Chemistry Department and Materials Sciences Institute, University of Seville-CSIC, Sevilla, 41092, Spain.

[2] Department of Microbiology and Environmental Toxicology, University of California Santa Cruz, Santa Cruz, CA 95064, USA.

[3] Servicios Generales de Investigación XPS, Centro de Investigación, Tecnología e Innovación de la Universidad de Sevilla (CITIUS), Av. Reina Mercedes 4B, 41012, Sevilla, Spain.

[4] College of Environmental Science and Engineering, Beijing Forestry University, 35 Qinghua East Road, Haidian District, Beijing 100083, P. R. China

Table S1. Textural properties and elemental analysis ICP-OES.

Catalyst	S_{BET} ($m^2 \cdot g^{-1}$)	Pore volume ($cm^3 \cdot g^{-1}$)	Pore size (nm)	wt. %Cu	wt. %K	wt. %Pt
Cu(IMP)	61.2	0.19	10.1	5.1	-	-
CuK(IMP)	57.2	0.24	15	5.4	12.1	-
CuK(COP)	56.1	0.33	22.4	4.9	9	-
CuK@	57.1	0.24	11.2	5.1	11	-
PtCuK@	53.3	0.20	11.0	5.0	10.8	0.6

Table S2. UV-vis quantitation of plasmonic and oxygen-vacancy absorption regions. "Plasmon post-activation" was obtained by integrating the differential spectra in Figure 1 (A, C, E, G) after activation between 450-800 nm and normalizing by the catalyst with the largest area (dimensionless relative area). "Plasmon retention" was obtained by integrating the differential spectra in Figure 1 (B, D, F, H) after reaction between 450-800 nm and normalizing by the catalyst with the largest area (dimensionless relative area). "Oxygen vacancies post-activation" and "Oxygen vacancies retention" values were calculated analogously using the 350-400 nm window.

Catalyst	Plasmon post-activation (450-800 nm)	Plasmon retention (450-800 nm)	Oxygen vacancies post-activation (350-400 nm)	Oxygen vacancies retention (350-400 nm)
Cu(IMP)	1	1	0.7	0
CuK(IMP)	0	1	1	1
CuK(COP)	0.9	0.6	0.9	1
CuK@	0.8	1	0.8	1

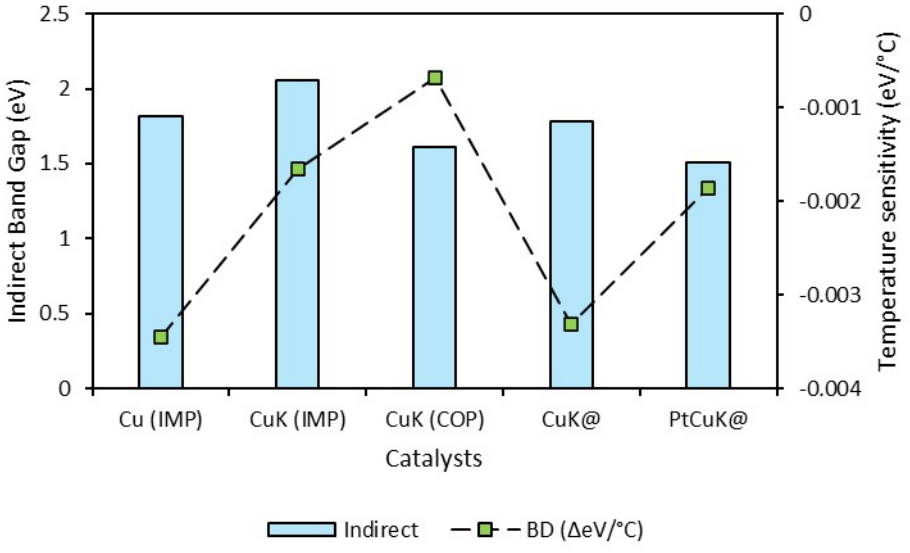

Figure S1. Indirect band gap calculated by Tauc analysis and temperature sensitivity calculated by indirect band gap evolution over temperature.

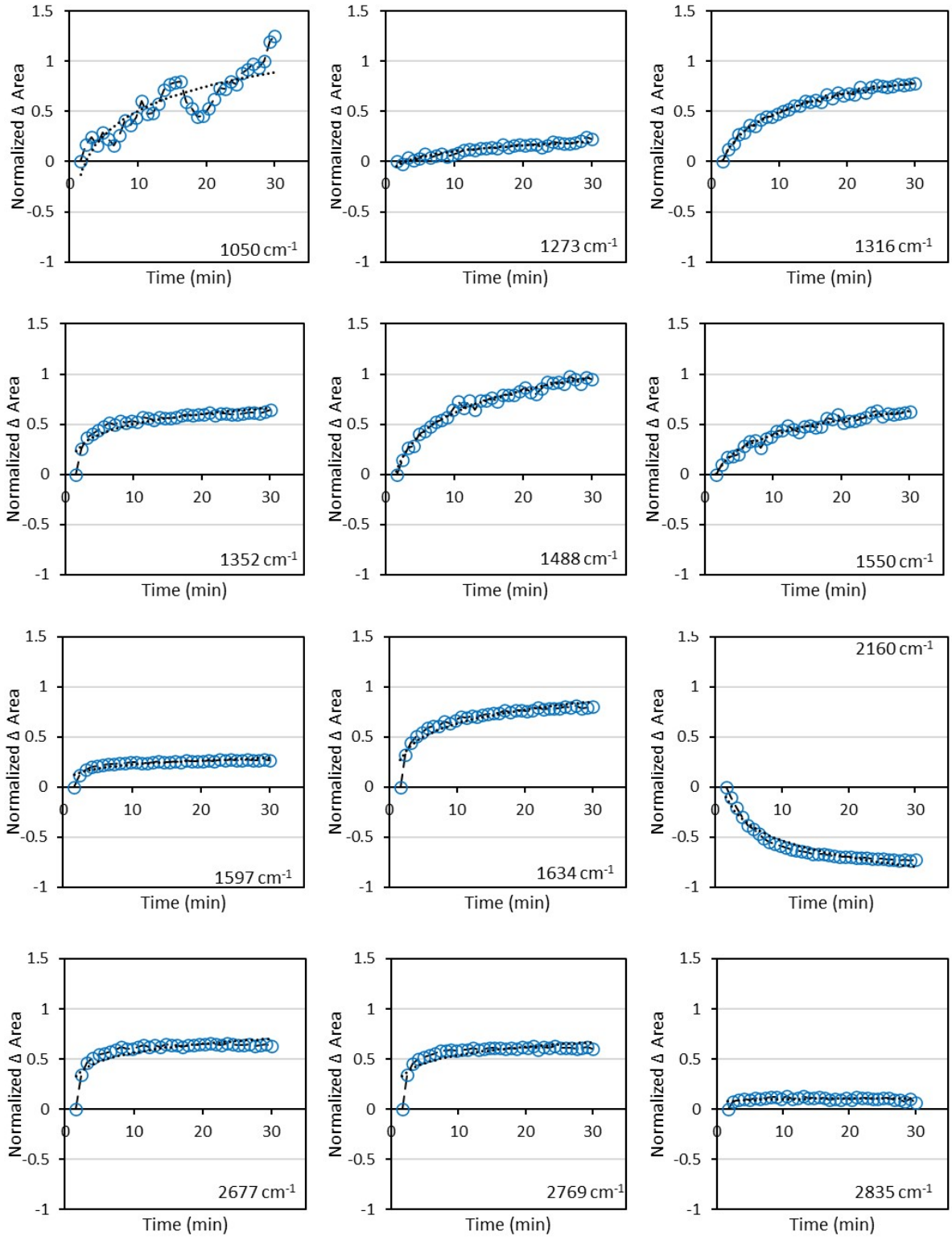

Figure S2. Relative growth respect to t=1min of deconvoluted DRIFTS bands for CuK@. Relative Δ Area for each band was estimated as ($Area_{t=imin}$ - $Area_{t=1min}$)/$Area_{t=1min}$. DRIFTS experiment was conducted at T= 250 °C, $4H_2$:$1CO_2$:1Ar, GHSV= 60L g^{-1} h^{-1}.

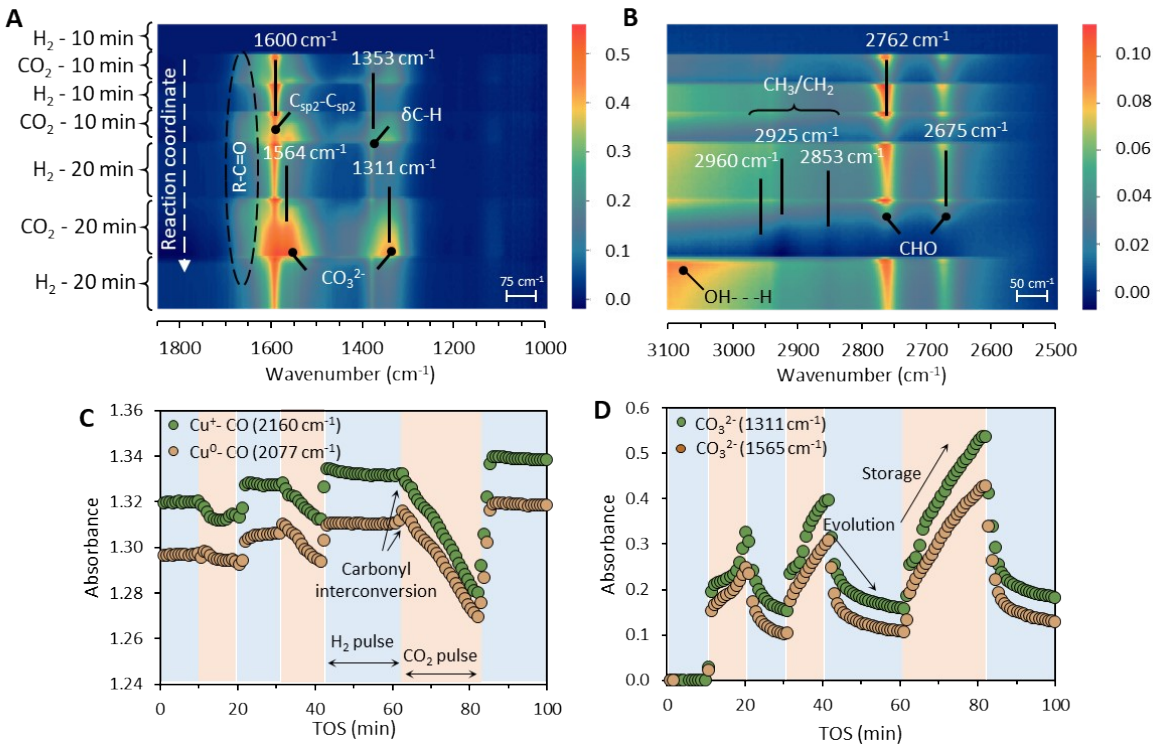

Figure S3. DRIFTS of CuK@ catalyst during pulse experiments. **A)** Heatmap of the 1000-1850 cm^{-1} during H_2/CO_2 pulse experiment. **B)** Heatmap of the 2500-3100 cm^{-1} region during H_2/CO_2 pulse experiment. **C)** Carbonyl bands evolution during H_2/CO_2 pulse experiment. **D)** Carbonates bands during H_2/CO_2 pulse experiment.

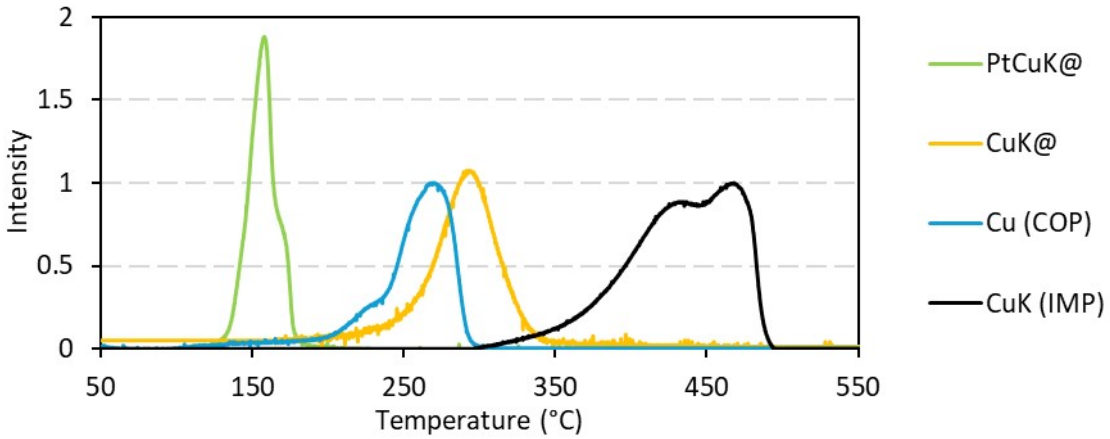

Figure S4. TPR for different catalyst formulations reveals that Pt promotion on CuK@ significantly reduces the temperature required to complete the redox cycle.

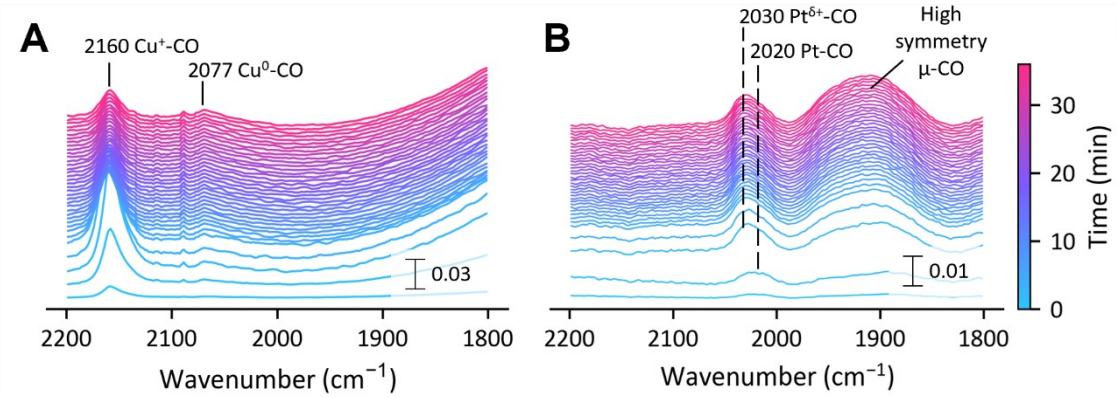

Figure S5. *Operando* DRIFTS spectra (carbonyl region, 2200-1800 cm^{-1}) during RWGS reaction over CuK@ (A) and PtCuK@ (B). On CuK@, the number of surface-bound carbonyls decreases over time, but it does not on PtCuK@. On PtCuK@, carbonyls are stabilized over Pt and destabilized over Cu. The blueshift over time observed for the Pt-CO carbonyl band indicates decreased electron density on Pt, which may be due to PtCu alloy formation and/or removal of superficial carbon [1,2]. DRIFTS experiment was conducted at T= 250 °C, $4H_2$:$1CO_2$:1Ar, GHSV= 60L g^{-1} h^{-1}.

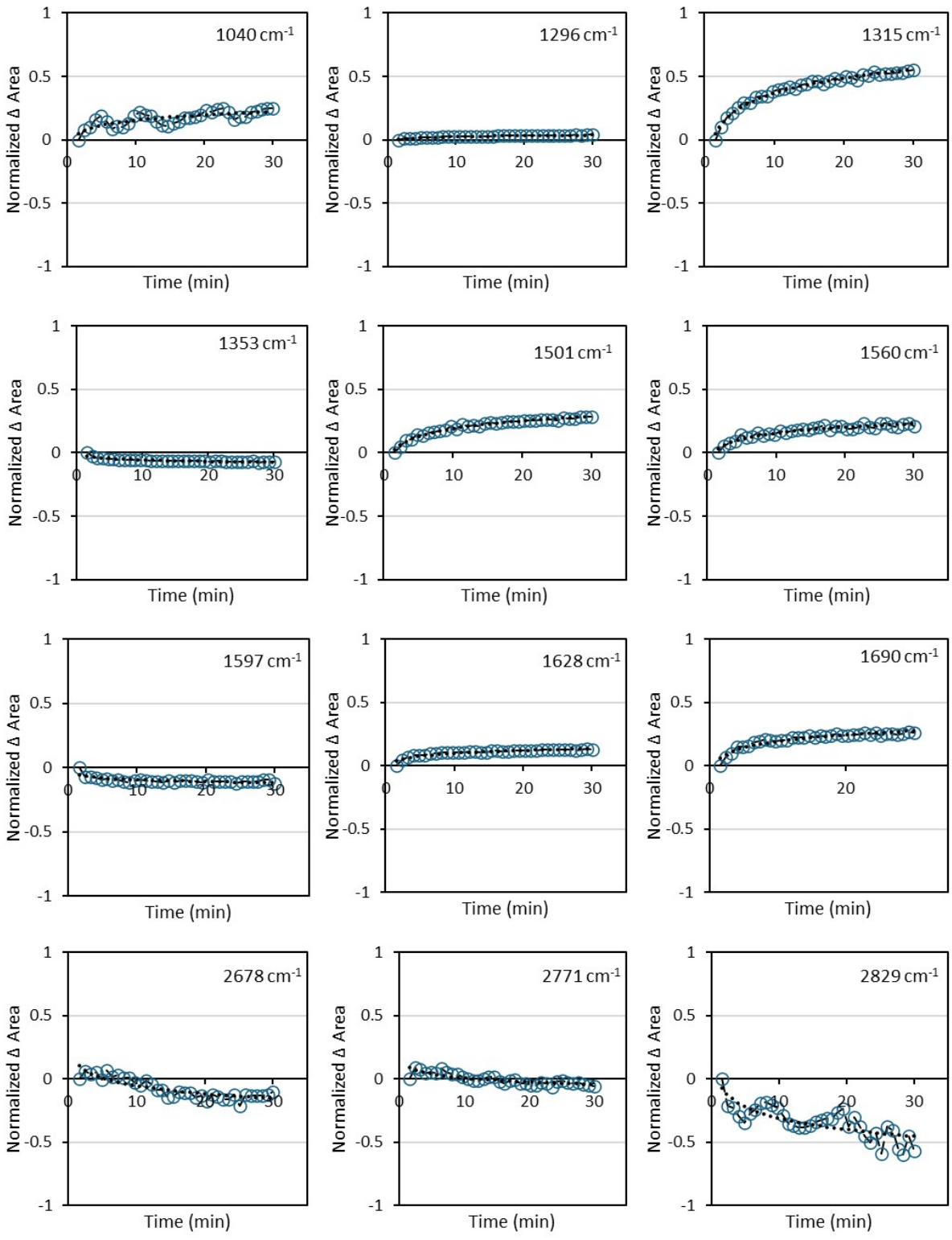

Figure S6. Relative growth respect to t=1min of deconvoluted DRIFTS bands for PtCuK@. Relative growth for each band was estimated as ($Area_{t=imin}$ - $Area_{t=1min}$)/$Area_{t=1min}$. DRIFTS experiment was conducted at T= 250 °C, $4H_2$:$1CO_2$:1Ar, GHSV= 60L g^{-1} h^{-1}.

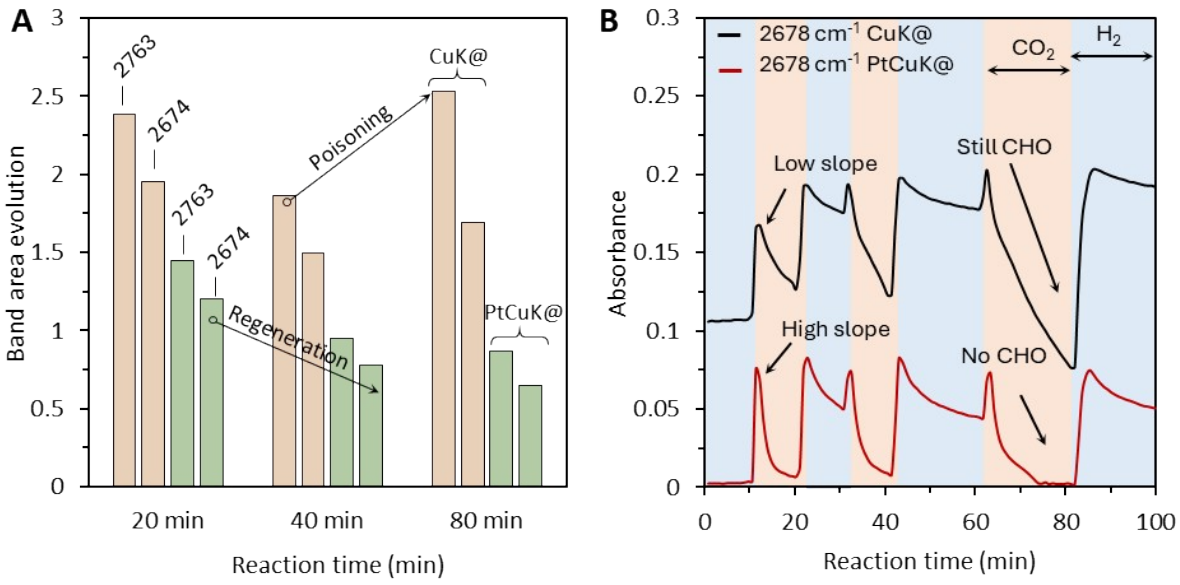

Figure S7. Coking precursor species (CHO) accumulated over CuK@ but not over PtCuK@ during pulse experiments. **A)** Evolution of CHO band area at the beginning of each CO_2 pulse. **B)** Evolution of CHO bands during pulse experiment. Y-axis values have been shifted to facilitate comparison.

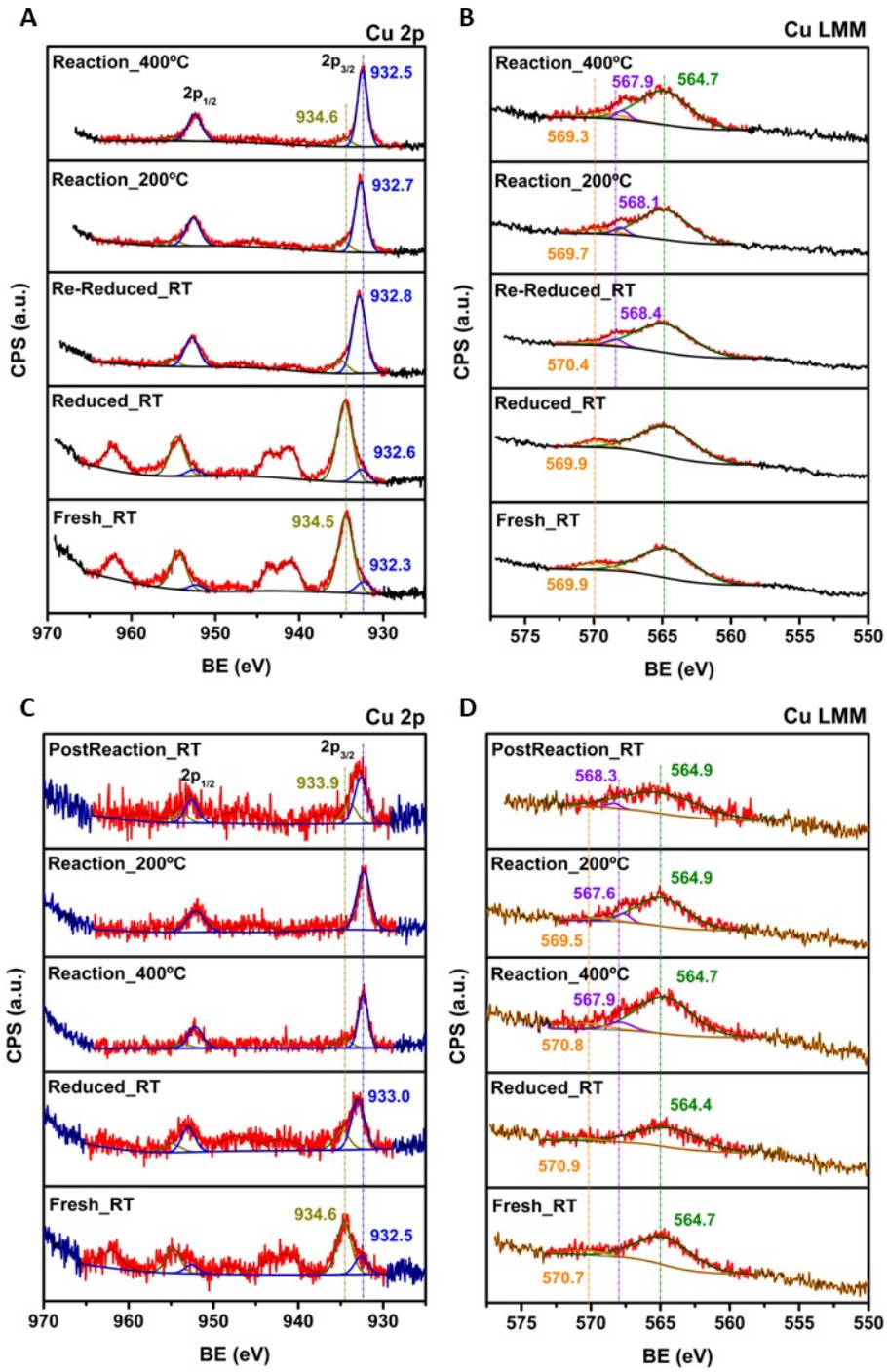

Figure S8. Oxidized (934.5 eV) and reduced (933 eV) Cu is observed in the fresh sample. Reduction and reaction processes revealed reduced Cu as the major component. **A)** Cu 2p for CuK@. **B)** Cu LMM for CuK@. **C)** Cu 2p for PtCuK@. **D)** Cu LMM for PtCuK@.

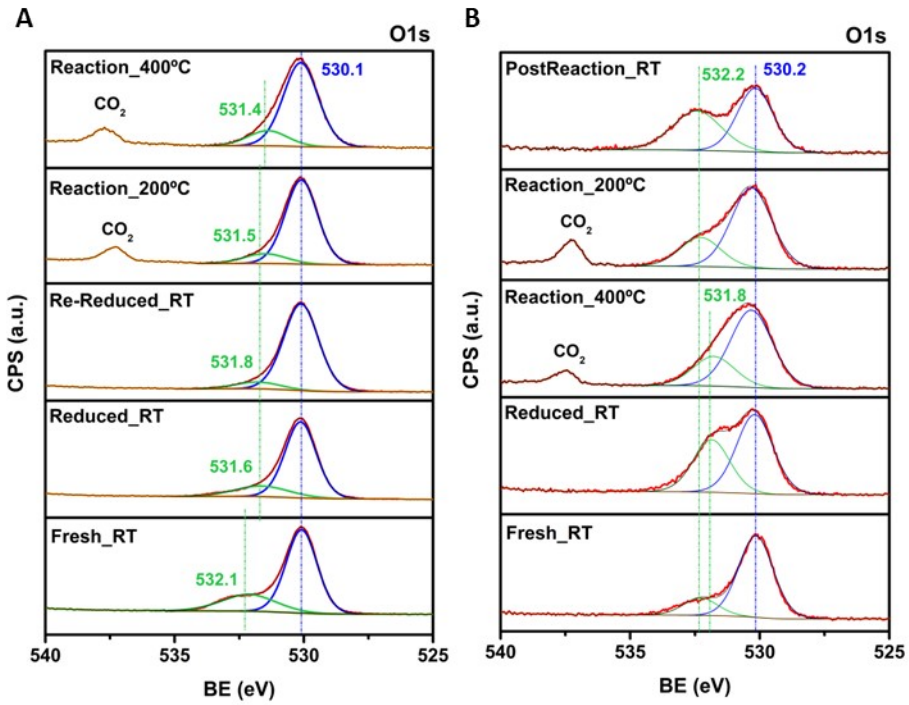

Figure S9. Two types of oxygen are observed: TiO2 (530.1 eV) and OH (532.1 eV). OH signal is higher in PtCuK@ **A)** O-1s NAP-XPS for CuK@. **B)** O-1s NAP-XPS for PtCuK@.

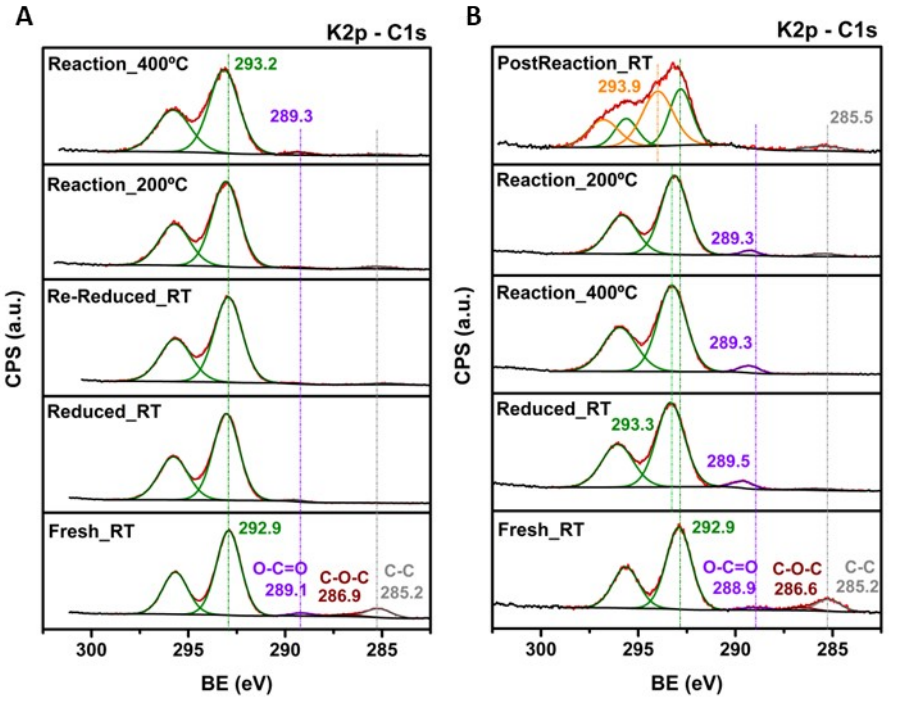

Figure S10. K signal (293.2 eV) is barely affected during the experiment. In PtCuK@ Ti-K interaction (293.9 eV) is observed due to titanates formation. Titanates are believed to facilitate spillover centers with carbon deposits. Carbon signal reveals different carbonaceous species which are highly sensible to reducing conditions. **A)** K-2p and C-1s NAP-XPS for CuK@. **B)** K-2p and C-1s NAP-XPS for PtCuK@.

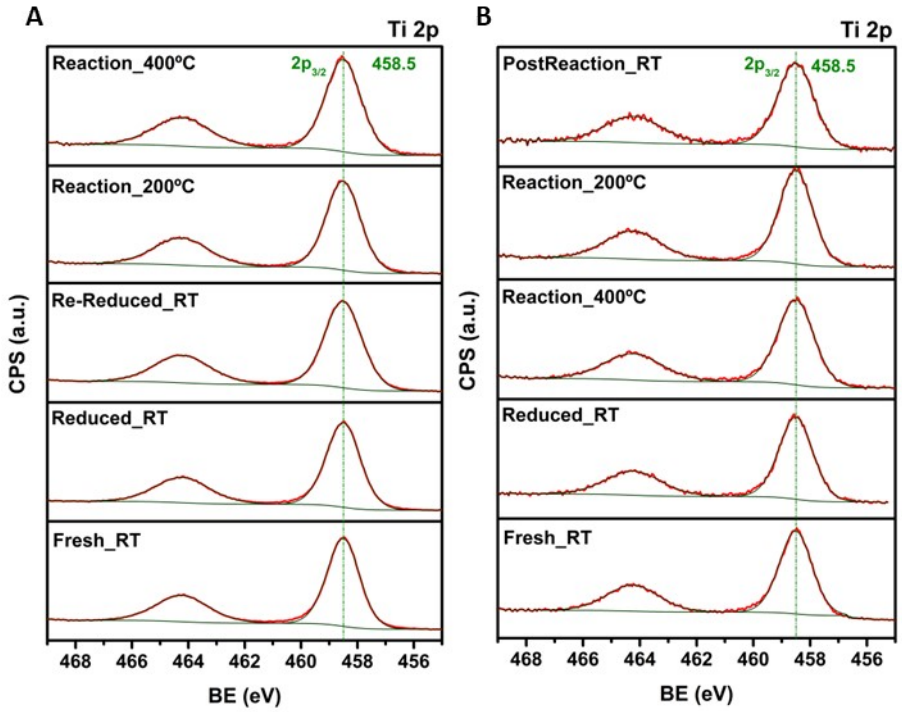

Figure S11. Ti signal (458.5 eV) was used for charge effect calibration. **A)** Ti-2p NAP-XPS for CuK@. **B)** Ti-2p NAP-XPS for PtCuK@.

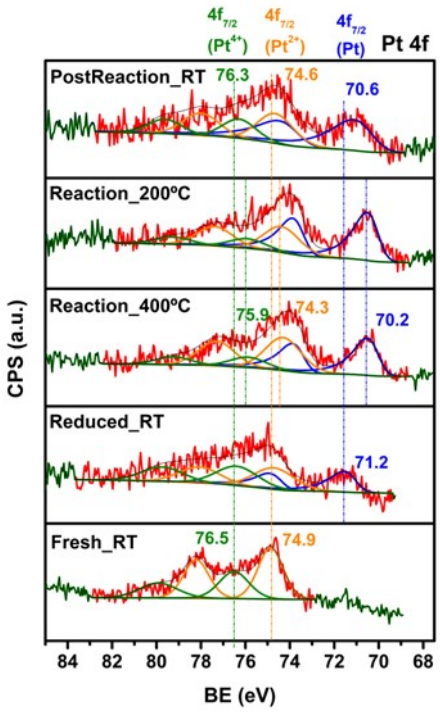

Figure S12. Three different types of Pt were observed during reaction, suggesting a highly active participation of Pt within the catalyst. Pt-4f NAP-XPS for PtCuK@.

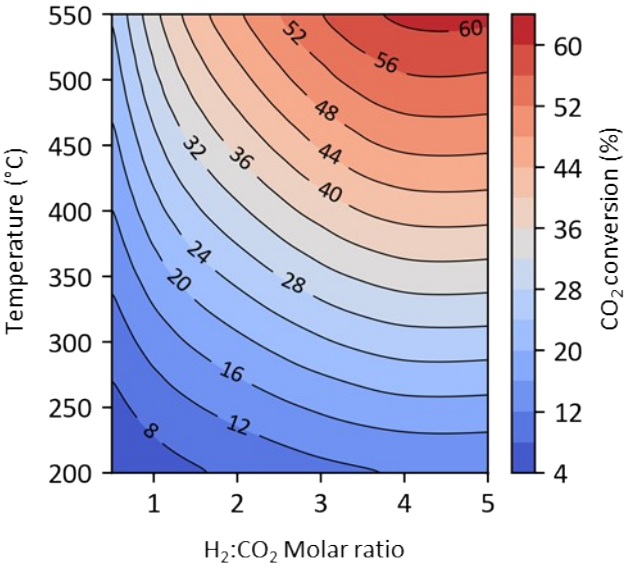

Figure S13. Isocontours for the thermodynamic equilibrium of RWGS from T=200 °C to T=550 °C and H_2:CO_2 molar ratio from 0.5 to 5 calculated by cubic splines interpolation over data generated on HSC6 Chemistry.

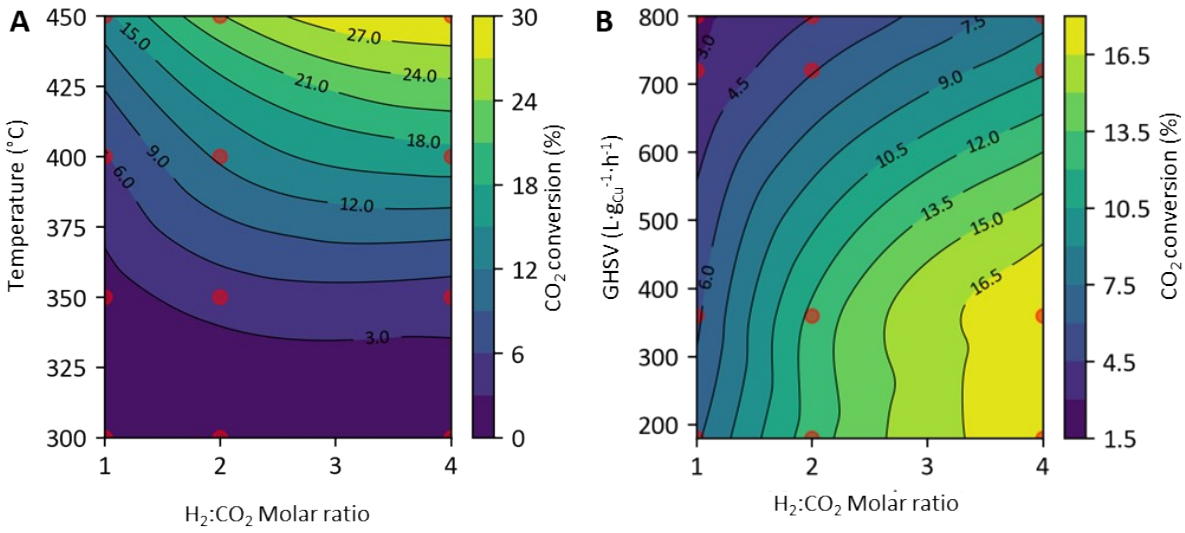

Figure S14. A) Isocontours for generated by cubic splines of CO_2 conversion on CuK@ modifying temperature and molar ratio with GHSV= 360 $L \cdot g_{Cu}^{-1} \cdot h^{-1}$. Red dots represent experimental data measurements. B**)** Isocontours for generated by cubic splines of CO_2 conversion on CuK@ modifying GHSV and molar ratio with T= 400 °C. Red dots represent experimental data measurements.

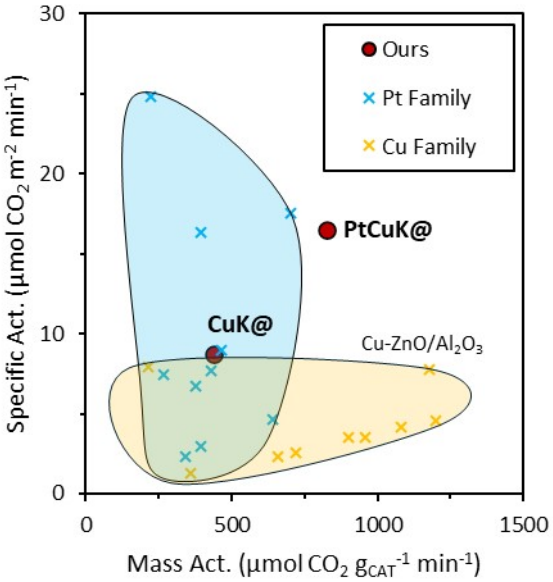

Figure S15. Specific activity comparison of CuK@ and PtCuK@ with Pt catalysts and Cu catalysts at T=400 °C (see Table S2).

Table S3. Comparison of catalysts reported in the literature and from this work.

Catalyst	T (°C)	H_2:CO_2	X CO_2 (%)	CO selectivity (%)	Specific activity µmol CO_2/(g_{cat}·min)	Specific activity µmol CO_2/(m^2·min)	Ref
PtCuK@	300	4	13.1	100	292.4	5.8	This work
PtCuK@	350	4	22.5	100	502.2	10.0	This work
PtCuK@	400	4	37	100	825.9	16.5	This work
PtCuK@	450	4	48.7	100	1087.1	21.7	This work
CuK@	400	4	19.6	100	437.5	8.8	This work
CuK@	450	4	31.1	100	694.2	13.9	This work
Pt/Al2O3	300	1.5	6	-	107.1	0.7	[3]
Pt/Al2O3	400	1.5	19	-	339.3	2.3	[3]
Pt/Al2O3	500	1.5	31	-	553.6	3.8	[3]
Pt/Al2O3	600	1.5	41	-	732.1	5.0	[3]
Pt/TiO2	300	1.5	15	-	267.9	2.0	[3]
Pt/TiO2	400	1.5	22	-	392.9	3.0	[3]
Pt/TiO2	500	1.5	37	-	660.7	5.0	[3]
Pt/TiO2	600	1.5	42	-	750.0	5.7	[3]
Pt-MCF-17	500	4	13.3	95.1	395.8	0.8	[4]
L-PtCo/MCF-17	500	4	12.6	98.2	375.0	0.9	[4]
M-PtCo/MCF-17	500	4	33.5	98.4	997.0	2.2	[4]
H-PtCo/MCF-17	500	4	19.8	99.2	589.3	1.3	[4]
Pt/MnO	400	4	26.84	97.7	639.0	4.7	[5]
Pt/SiO2	350	2	9.0	96.6	176.0	-	[5]
Pt/TiO2	350	2	10.2	100	367.7	2.5	[6]
Pt-TiO2 (A)	300	4	5.5	100	98.2	10.9	[7]
Pt-TiO2 (A)	400	4	12.5	100	223.2	24.8	[7]
Pt-TiO2 (A)	500	4	30	100	535.7	59.5	[7]
Pt-TiO2 (A)	600	4	40	100	714.3	79.4	[7]
Pt-TiO2 (G)	300	4	15	100	267.9	5.2	[7]
Pt-TiO2 (G)	400	4	26	100	464.3	8.9	[7]
Pt-TiO2 (G)	500	4	35	100	625.0	12.0	[7]
Pt-TiO2 (G)	600	4	45	100	803.6	15.5	[7]
Pt/TiO2 (U)	300	4	12	100	214.3	3.8	[7]
Pt/TiO2 (U)	400	4	21	100	375.0	6.7	[7]
Pt/TiO2 (U)	500	4	31	100	553.6	9.9	[7]
Pt/TiO2 (U)	600	4	42	100	750.0	13.4	[7]
Pt/TiO2 (M)	300	4	10	100	178.6	7.4	[7]
Pt/TiO2 (M)	400	4	22	100	392.9	16.4	[7]
Pt/TiO2 (M)	500	4	32	100	571.4	23.8	[7]
Pt/TiO2 (M)	600	4	42.5	100	758.9	31.6	[7]
Pt/TiO2 (D)	300	4	9	100	160.7	4.5	[7]
Pt/TiO2 (D)	400	4	15	100	267.9	7.4	[7]
Pt/TiO2 (D)	500	4	32.5	100	580.4	16.1	[7]
Pt/TiO2 (D)	600	4	42.2	100	753.6	20.9	[7]
Pt/TiO2 (S)	300	4	15	100	267.9	4.8	[7]
Pt/TiO2 (S)	400	4	24	100	428.6	7.7	[7]
Pt/TiO2 (S)	500	4	36	100	642.9	11.5	[7]
Pt/TiO2 (S)	600	4	41.5	100	741.1	13.2	[7]
Au/TiO2	200	9	6	-	67.0	1.4	[8]
Au/TiO2	225	9	11	-	122.8	2.5	[8]
Au/TiO2	250	9	16	-	178.6	3.6	[8]
Au/TiO2	275	9	24	-	267.9	5.5	[8]
Au/TiO2	300	9	30	-	334.8	6.8	[8]

Au/TiO2	325	9	36	-	401.8	8.2	[8]
Au/TiO2	350	9	40	-	446.4	9.1	[8]
Au/TiO2	375	9	45	-	502.2	10.2	[8]
Au/TiO2	400	9	47	-	524.6	10.7	[8]
PtCs/TiO2	400	4	21	100	703.1	17.6	[9]
3CuAl	400	4	-	100	360.0	1.3	[10]
5CuAl	400	4	-	100	660.0	2.4	[10]
8CuAl	400	4	-	100	720.0	2.6	[10]
10CuAl	400	4	-	100	960.0	3.5	[10]
12CuAl	400	4	-	100	1080.0	4.1	[10]
15CuAl	400	4	-	100	900.0	3.5	[10]
12CuAl-GD	400	4	-	100	1200.0	4.5	[10]
Cu/CeO2	400	4	32	100	214.3	7.9	[11]

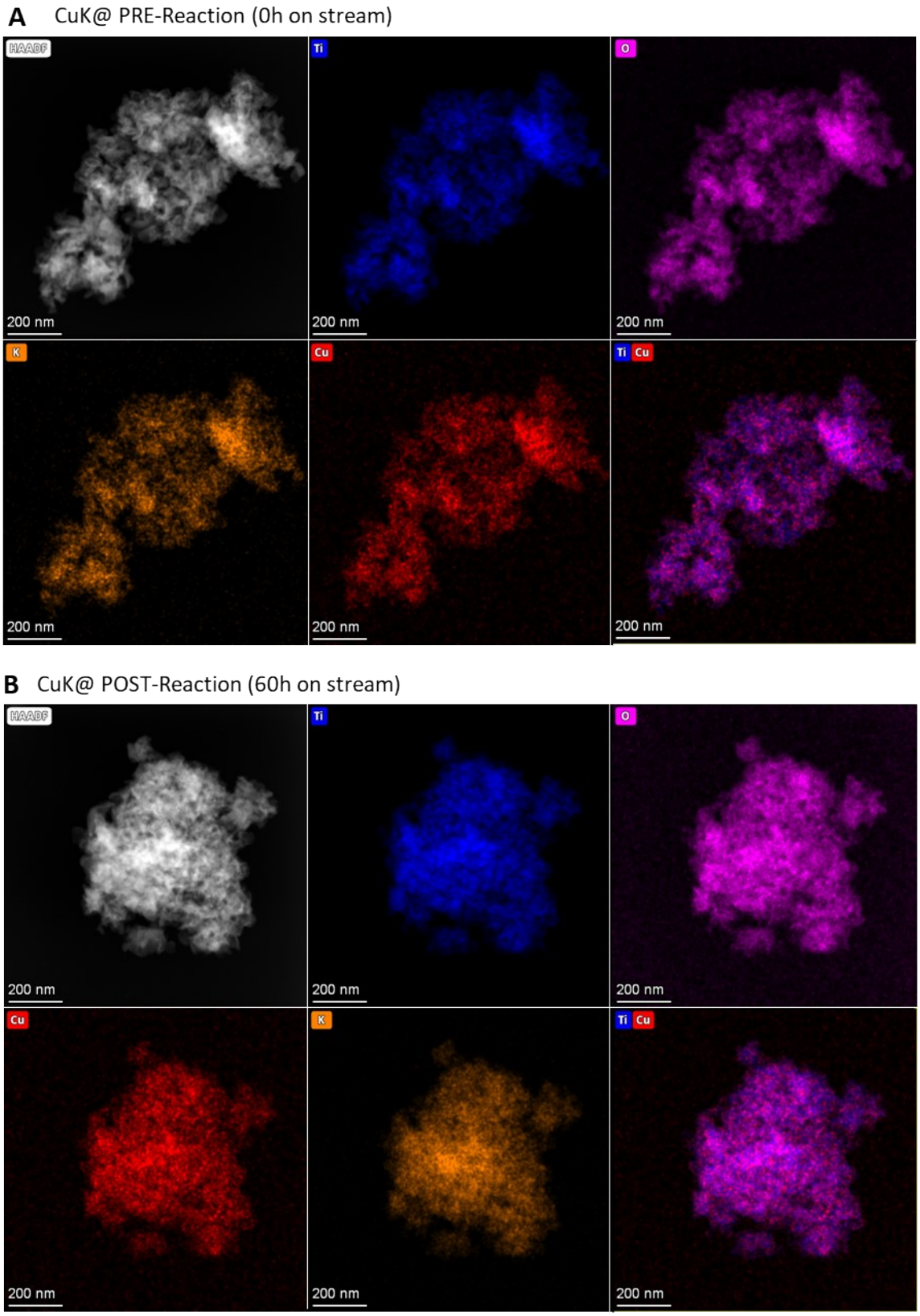

Figure S16. HAADF-STEM images of CuK@. **A)** Images before long-term testing (t= 0h). **B)** Images after long-term testing (t= 60h).

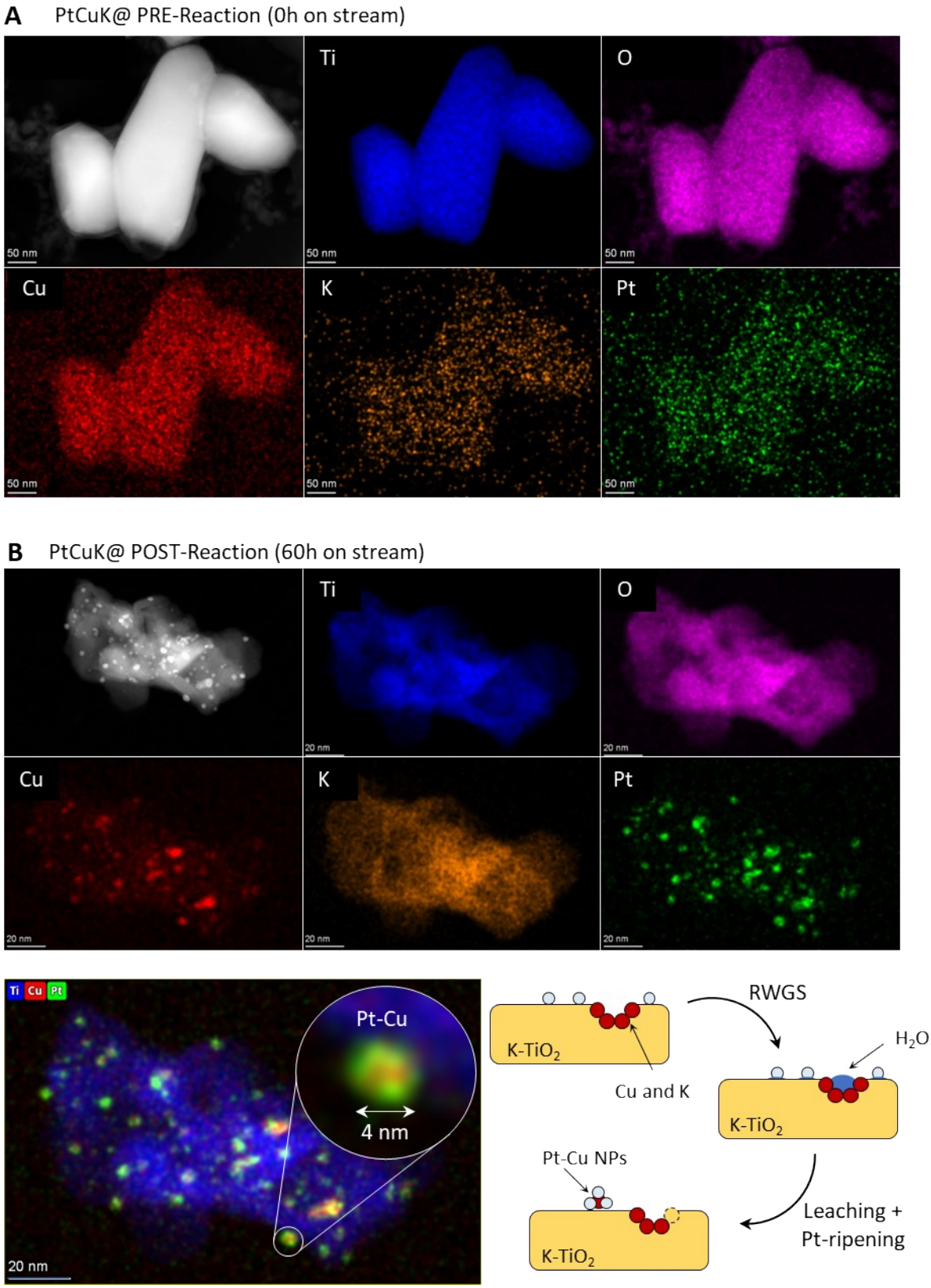

Figure S17. HAADF-STEM images of CuK@. **A)** Images before long-term testing (t= 0h). **B)** Images after long-term testing (t= 60h). Detail of PtCu alloy formed after reaction where leaching and ripening processes are believed to be responsible of catalyst ageing.

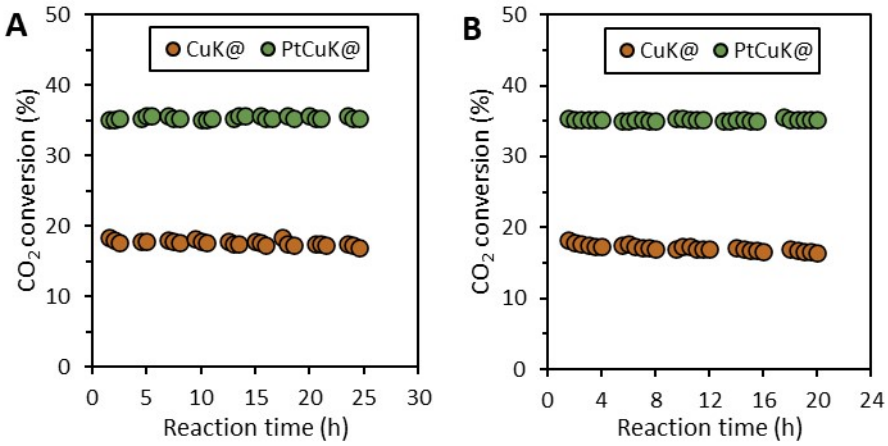

Figure S18. Regeneration and recyclability tests (i.e., 1.5 hours in a H_2:N_2 atmosphere at 400 °C) and recyclability (x hours in reaction atmosphere, T = 400°C, GHSV = 360 $L \cdot g_{Cu}^{-1} \cdot h^{-1}$, H_2:CO_2= 4). **A)** 1.5-hour regeneration followed by 1.5 hours under reaction conditions for a total of 9 cycles. **B)** 1.5-hour regeneration followed by 3 hours under reaction conditions for a total of 5 cycles.

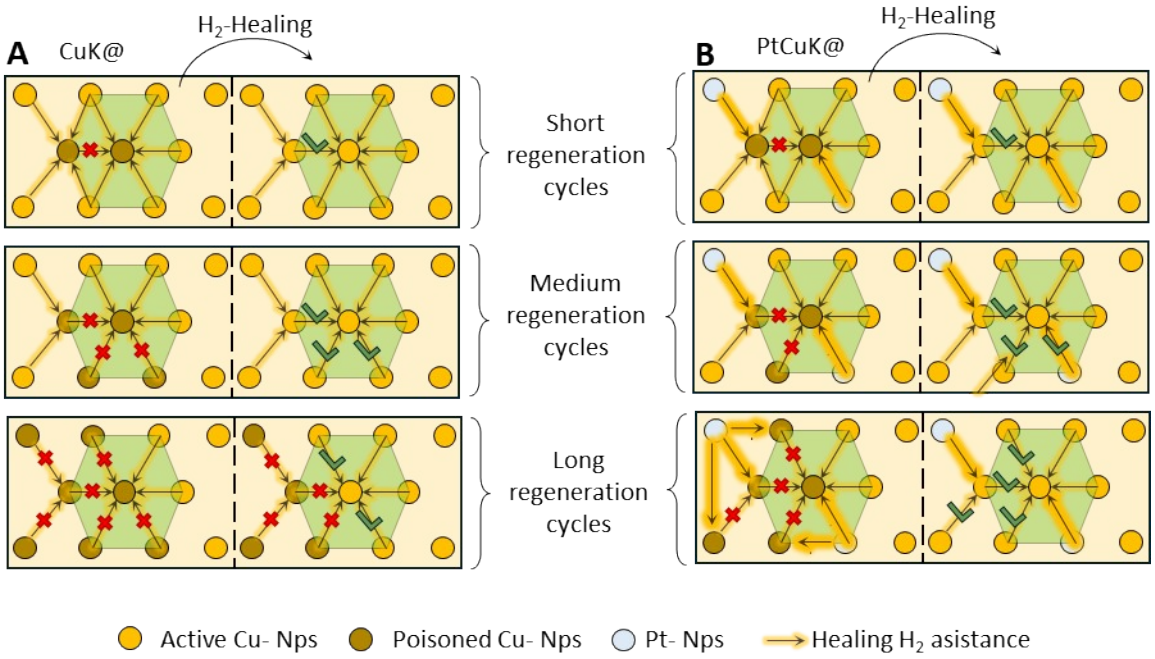

Figure S19. Proposed regeneration mechanisms for CuK@ and PtCuK@ catalysts. Surface spillover capacity is believed to be a critical factor in the regeneration of active sites. The authors suggest that a high population of surface H* species is key to preventing the accumulation of stable and unreactive adducts on the active centers, which would otherwise hinder the regeneration of the essential metallic species in the catalytic cycle. The formation of inert adducts is particularly notable during extended reaction times with CuK@, where the efficiency of the catalytic cycle becomes significantly compromised. Pt incorporation hinders adduct formation by boosting H_2 spillover and regenerating metallic centers. **A)** Regeneration mechanism for CuK@. **B)** Regeneration mechanism for PtCuK@.

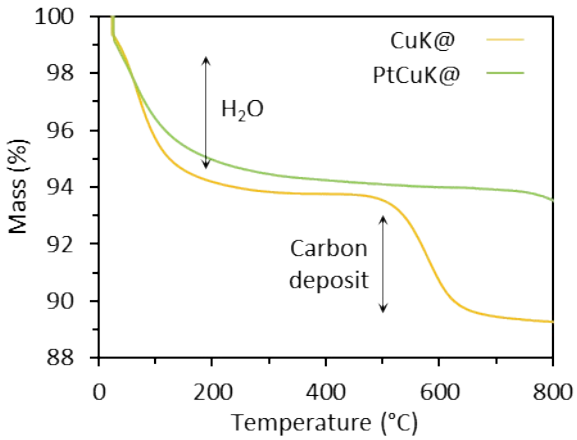

Figure S20. Thermogravimetric analysis of PtCuK@ and CuK@ after 8 long cycles revealed coke deposits on CuK@ that were associated with deactivation. PtCuK@ did not show any apparent deposit.

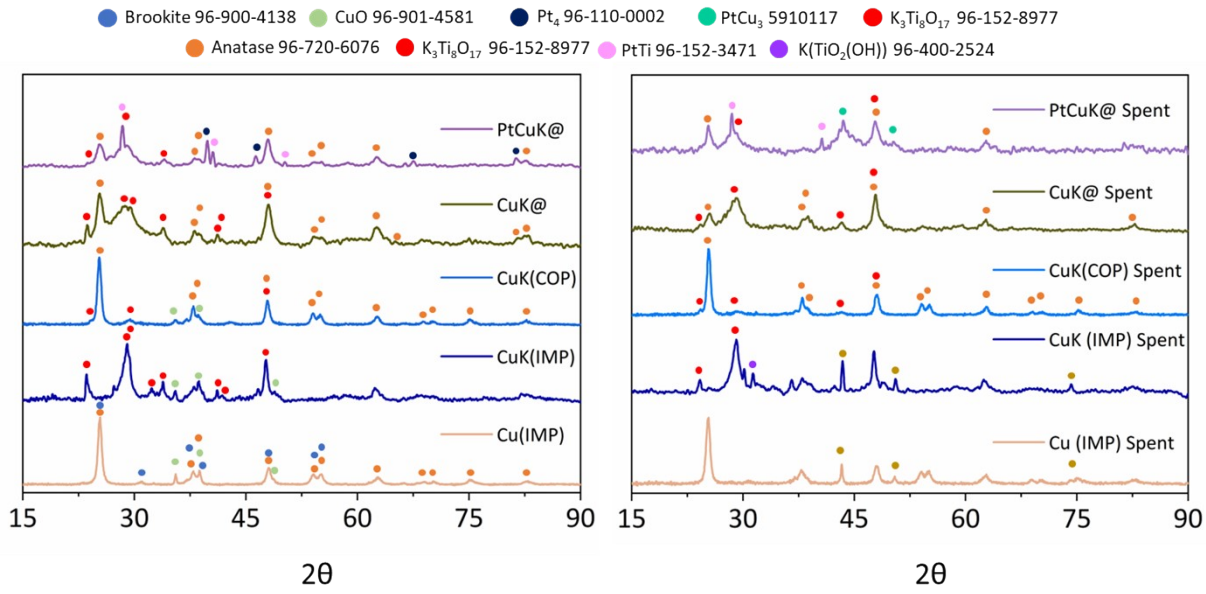

Figure S21. XRD of fresh and post-reaction (CO_2 conversion between 300 and 450 °C with GHSV= 360 L g_{Cu}^{-1} h^{-1}) catalysts.

References

1 H. Yoshida, S. Narisawa, S. Fujita, L. Ruixia and M. Arai, *Phys. Chem. Chem. Phys.*, 2012, **14**, 4724.

2 W. F. Lin, M. S. Zei and G. Ertl, *Chemical Physics Letters*, 1999, **312**, 1–6.

3 S. S. Kim, H. H. Lee and S. C. Hong, *Applied Catalysis A: General*, 2012, **423–424**, 100–107.

4 Á. Szamosvölgyi, Á. Pitó, A. Efremova, K. Baán, B. Kutus, M. Suresh, A. Sápi, I. Szenti, J. Kiss, T. Kolonits, Z. Fogarassy, B. Pécz, Á. Kukovecz and Z. Kónya, *ACS Appl. Nano Mater.*, 2024, **7**, 9968–9977.

5 I. Szenti, A. Efremova, J. Kiss, A. Sápi, L. Óvári, G. Halasi, U. Haselmann, Z. Zhang, J. Morales-Vidal, K. Baán, Á. Kukovecz, N. López and Z. Kónya, *Angew Chem Int Ed*, 2024, **63**, e202317343.

6 S. Kattel, B. Yan, J. G. Chen and P. Liu, *Journal of Catalysis*, 2016, **343**, 115–126.

7 S. S. Kim, H. H. Lee and S. C. Hong, *Applied Catalysis B: Environmental*, 2012, **119–120**, 100–108.
8 V. Kyriakou, A. Vourros, I. Garagounis, S. A. C. Carabineiro, F. J. Maldonado-Hódar, G. E. Marnellos and M. Konsolakis, *Catalysis Communications*, 2017, **98**, 52–56.
9 G. Torres-Sempere, R. Blay-Roger, L. A. Luque-Álvarez, J. L. Santos, L. F. Bobadilla, L. Pastor-Pérez, M. A. Centeno, W. Y. Hernández, I. Yousef, J. A. Odriozola and T. R. Reina, *J. Mater. Chem. A*, 2024, **12**, 1779–1792.
10 X. Ai, H. Xie, S. Chen, G. Zhang, B. Xu and G. Zhou, *International Journal of Hydrogen Energy*, 2022, **47**, 14884–14895.
11 M. Li, T. H. My Pham, Y. Ko, K. Zhao, L. Zhong, W. Luo and A. Züttel, *ACS Sustainable Chem. Eng.*, 2022, **10**, 1524–1535.